INORGANIC CHEMISTRY FRONTIERS

RESEARCH ARTICLE

View Article Online
View Journal | View Issue

Cite this: *Inorg. Chem. Front.*, 2025, **12**, 569

Unveiling the role of surface iodine vacancies in $CsPbI_3$ perovskite: carrier recombination dynamics and defect passivation mechanisms†

Jing Wang * and Xiang-Mei Duan

Lead–iodine perovskites are emerging as promising candidates for next-generation solar cells, yet a divergence persists between the theoretical and experimental realms regarding the impact of surface iodine vacancies (V_I) on device performance. To elevate cell efficiency, a profound understanding and delicate control of V_I and their passivation mechanisms are crucial. In this work, we studied various V_I defects near the surface of all-inorganic $CsPbI_3$ perovskite using *ab initio* non-adiabatic molecular dynamics. The results show that the electron–hole (e–h) recombination lifetime highly depends on the defect positions and configurations, as well as the efficacy of Lewis base additives in passivating defects. Despite the outermost layer V_I creating no defect state within the band gap, the carrier recombination rate accelerates significantly by a factor of 2 compared to that with the defect-free surface, owing to strong electron–phonon coupling. Subsurface defects create a localized hole trapping state, enabling swift capture of valence band holes, which subsequently accelerate recombination with the conduction band electrons by a factor of 6.5. Remarkably for Pb-dimers, this rate escalates 13-fold. Incorporating the Lewis base molecule $HCOO^-$ forms the stable Pb–O bonds with lead ions, preventing surface V_I reconstruction (iodine migration), Pb-dimer formation, and an in-band defect state. These effectively reduce the electron–phonon coupling, achieving performance comparable to that of the defect-free surface. This work reconciles contradictory of surface V_I on perovskite performance, and enriches our understanding of surface defect properties and their effects on carrier dynamics and device efficiency.

Received 9th October 2024,
Accepted 30th November 2024

DOI: 10.1039/d4qi02533d

rsc.li/frontiers-inorganic

Introduction

All-inorganic $CsPbI_3$ perovskite has attracted much attention in recent years due to its superb optoelectronic properties, such as the high defect tolerance, strong optical absorption, long carrier lifetime, and remarkable thermal stability. These combined factors have propelled the power conversion efficiency (PCE) from an initial 1.7% (reported by Eperon *et al.*)[1] to over 21%[2–4] within a decade, underscoring its immense potential as a next generation candidate of low-cost solar cells. However, despite these achievements, the PCE of $CsPbI_3$ still lags behind that of organic–inorganic hybrid perovskites (OIHPs) of 26.7%,[5] and is far from the theoretical limit of 30% predicted by Shockley–Queisser.[6] This difference is attributed to the charge capture and recombination of photogenerated carriers, which hinders further efficiency gains. These issues are closely linked to defects in $CsPbI_3$ cell, as they often involve some negative effects such as non-radiative recombination, charge capture and scattering, and ion migration. Experimental reports show that surface defect concentration in perovskites is 2–3 orders of magnitude higher than that of bulk defects,[7–9] and the iodine vacancy (V_I) is a pivotal defect because of its low formation energy.[10–13] Therefore, enhancing cell PCE relies on a profound comprehension and delicate control of the properties and passivation of V_I.

Despite the abundance of theoretical studies investigating the electrical properties of V_I on perovskite surfaces, the majority have focused on the outermost layer, which is often classified as a benign defect. For example, Uratani *et al.* found that V_I on MAI- and PbI_2-terminated surfaces of $MAPbI_3$ do not introduce any new impurity states within the band gap.[14] Ambrosio *et al.* calculated the formation energies of surface defects and determined that the charge transition level of V_I resides in the conduction band (CB).[10] Apart for OIHPs, all-inorganic perovskites exhibit analogous characteristics. Nenon

School of Physical Science and Technology, Ningbo University, Ningbo, 315211, P.R. China. E-mail: wangjing4@nbu.edu.cn

†Electronic supplementary information (ESI) available: Computational details on coupled kinetic equations, absorption energy, evolution of Pb–Pb distances around V_I defects on the subsurface; spin-polarized calculations of electronic structures on the V_I^{Sur} defect; population evolution of key states. See DOI: https://doi.org/10.1039/d4qi02533d

et al. reported that surface V_I defects in $CsPbI_3$ form shallow-level states near the CB.[15] According to Shockley–Read–Hall (SRH) theory,[16,17] such defects are unlikely to serve as effective e–h recombination centers, and may even contribute positively to the generation of photogenerated carriers. Therefore, passivating surface V_I may not be essential for enhancing carrier lifetime and device performance.

Nevertheless, increasing experimental evidences underscore the significant role of passivating surface defects, particularly V_I, in enhancing the optoelectronic properties of lead-iodide perovskites.[18–23] For instance, Wang *et al.* found that an active passivator with dynamic covalent bonds under the influence of water and heat factors can release additional Lewis bases, effectively repair the surface V_I of the $APbI_3$ perovskite and increase PCE to 25.1%.[22] Pan *et al.* introduced $EDAI_2$ as a surface modifier to eliminate surface V_I in Pb–Sn mixed perovskites, prolonging carrier lifetime and achieving a PCE of 23.32%.[23] Li *et al.* applied MFA molecules to all-inorganic perovskites to achieve anion-fixation and uncoordinated-Pb passivation, suppress Pb and I ion migration, reduce defect concentration, and attain a maximum PCE of 22.14% for $CsPbI_{3-x}Br_x$.[13] These findings suggest that modified surface V_I defects indeed play a pivotal role in mitigating carrier recombination and energy loss, hinting at their function as effective charge recombination centers. This apparent paradox—V_I defects being considered benign theoretically yet detrimental experimentally—necessitates a deeper understanding of surface V_I defect properties and their impact on device performance from the perspective of carrier dynamics.

In this work, we employed first-principles defect calculations, CI-NEB simulations, time-domain density functional theory (TD-DFT) and non-adiabatic molecular dynamics (NAMD) to systematically investigate various V_I near the $CsPbI_3$ (001) surface. We analyzed the geometric and electronic structures of these defects before and after passivation with $HCOO^-$, a typical Lewis base molecule. Additionally, we offer a detailed examination of carrier capture and non-radiative e–h recombination processes associated with these defects. Our results reveal that the outermost layer V_I (named V_I^{Sur}) may coexist with the subsurface V_I defects due to their negligible energy difference (35 meV). The subsurface V_I exhibit two distinct defect structures: Pb-nondimer ($V_{I\text{-}N}^{Sub}$) and Pb-dimer ($V_{I\text{-}D}^{Sub}$) configurations. Notably, CI-NEB results show that these three defects possess low migration barriers compared with OIHPs, revealing a higher propensity for ion migration or defect reconstruction on the $CsPbI_3$ surface. Despite V_I^{Sur} creating no defect states (DS) within the band gap, the e–h recombination lifetime across the conduction band minimum (CBM) and valence band maximum (VBM) is reduced by half, mainly due to the stronger non-adiabatic coupling (NAC) compared with perfect surface. This demonstrates that V_I^{Sur} is a detrimental defect that accelerates carrier recombination. For $V_{I\text{-}N}^{Sub}$, it forms a hole trap state below the CBM, which increases the carrier recombination channels, enhances NAC and accelerates e–h recombination by a factor of 6.5 (compared to the pristine system). For $V_{I\text{-}D}^{Sub}$, this effect is even more pronounced. Free holes in the valence band are strongly trapped by the mid-gap DS, resulting in an acceleration of the recombination rate by a factor of 13. The passivator $HCOO^-$ forms stable Pb–O bonds with the unsaturated-Pb ions near V_I, effectively prevents Pb-dimer formation, eliminates deep DS, and inhibits iodine migration. Furthermore, it mitigates free carrier recombination at band edges, comparable to that of the defect-free surface, due to weaken NAC and eliminate additional recombination channels. This work offers profound insights into the passivation mechanisms of detrimental surface V_I by Lewis base molecules, paving the way for enhancing solar cell efficiency.

Calculation methods

We utilized the Vienna *ab initio* Simulation Package (VASP) code[24,25] to perform geometric optimization, molecular dynamics and electronic structure calculations. The projector augmented wave (PAW)[26] was employed to handle interactions between the valence electrons and ion cores, and the exchange–correlation interaction is described by the generalized gradient approximation (GGA) with the Perdew–Burke–Ernzerhof (PBE) functional.[27] The lattice constants and atomic coordinates of β-phase $CsPbI_3$ are fully optimized using a plane-wave cutoff energy of 400 eV and a Γ-centered 4 × 4 × 3 Monkhorst–Pack (MP) mesh.[28] The convergence criteria for energy and force were set to 1×10^{-5} eV and 0.01 eV $Å^{-1}$, respectively. The optimized lattice constants were found to be $a = b = 8.84$ Å and $c = 12.94$ Å, in good agreement with the experimental values ($a = b = 8.78$ Å and $c = 12.33$ Å).[29]

Based on the optimized 2 × 2 × 1 bulk supercell, we constructed a five-layer (001) slab model terminated with CsI to investigate surface defects, as shown in Fig. 1. The reasons for choosing this model are as follows: firstly, both theoretical and experimental evidences demonstrate that the (001) surface

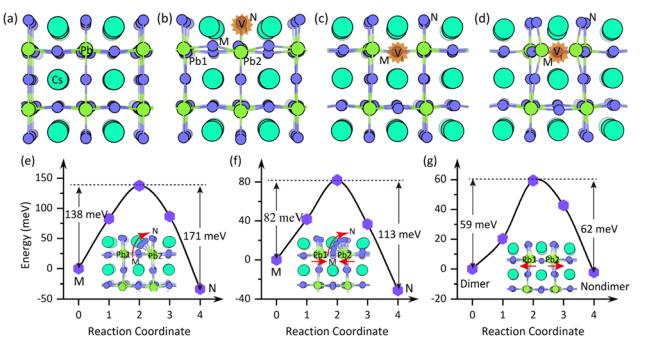

Fig. 1 Upper panel: optimized structures of (a) perfect $CsPbI_3$ surface, (b) surface defects with V_I in the outermost layer (henceforth referred to as the surface layer defect), and (c) Pb-nondimer and (d) Pb-dimer structures located on the subsurface, respectively. Lower panel: the transition barrier and migration process between different V_I defect structures. (e and f) The transition process between the surface layer defect and nondimer and dimer configurations, respectively. (g) The transition process between the subsurface defects.

exhibits higher stability compared to other orientations.[30,31] Secondly, a thickness of five layers is sufficient to ensure the accuracy of surface simulations.[32] Lastly, due to its lower surface energy, the CsI-terminated surface is more likely to be exposed on the material surface.[31–33] With these factors, we investigated the geometric configurations, electronic structures, and carrier dynamics of V_I on the CsI-terminated surface. To avoid coulombic interactions between periodic surfaces, the vacuum thickness was set to 15 Å. Considering the computational cost and the direct bandgap nature of $CsPbI_3$, we used a single *k*-point for geometric optimization and MD calculations, while a dense 5 × 5 × 1 MP mesh was employed for electronic structure analysis. Van der Waals interactions were accounted for using the DFT-D3 method.[34] The diffusion energy barrier of iodine ions (or V_I) was obtained by the CI-NEB method,[35] with a force convergence criterion of 0.08 eV $Å^{-1}$.

To investigate the carrier lifetime in the first-excited state, after structural optimization, we used a Nosé thermostat to simulate the canonical ensemble of the system and stabilized the temperature at 300 K.[36] Then, a 6 ps trajectory was obtained with a time step of 1 fs in the microcanonical ensemble, from which 3 ps was selected for subsequent non-adiabatic coupling (NAC) calculations. NAC was carried out using the Python eXtension for Ab Initio Dynamics (PYXAID)[37,38] combined with the Quantum Espresso (QE)[39] code. NAMD was conducted using the semiclassical decoherence-induced surface hopping (DISH) technique.[40] To achieve reliable statistical data for fitting carrier lifetime, we repeated the NAC data twice (three times for Pb-dimers) and generated 9000 (8000) hamiltonians, of which the first 3000 (2000) hamiltonians were used as the initial conditions.

Results and discussion

Fig. 1 depicts the optimized geometries of the pristine surface and V_I systems, along with calculated transition state dynamics between various defect configurations, using the perfect surface as the benchmark. We initially examined V_I located in the outermost layer (denoted as V_I^{Sur}), that is, by removing an I atom at the N-site, as shown in Fig. 1b. After relaxation, the structure exhibits two characteristics: firstly, the surface distortion is minimal, which is primarily attributed to the movement of I ions at the M-site along the *z*-direction towards the vacuum layer by 0.34 Å, stemming from V_I disrupting the original interionic forces and re-establishing a new equilibrium. Secondly, the average Pb1–Pb2 distance (6.24 Å) is almost identical to that of the perfect system (6.25 Å), indicating minimal influence on the I atoms at the M-site, which favors ion migration. When V_I are located in the subsurface, its structure becomes intricate, as evidenced by a 35 meV energy reduction compared to that at the surface, exemplified by the Pb-nondimer ($V_{I\text{-}N}^{Sub}$) in Fig. 1c and Pb-dimer ($V_{I\text{-}D}^{Sub}$) in Fig. 1d, respectively. The Pb-nondimer structure exhibits a shortened Pb distance of 5.61 Å due to the large space created by V_I, while the inorganic PbI_6 structure is maintained (Fig. 1c). Conversely, the Pb-dimer shows an elongated distance of 3.79 Å (exceeding the bulk value of 3.3 Å), attributed to reduced surface stress and a singly occupied bonding orbital electron weakening the electronic energy. Hence, the surface Pb-dimer is unstable compared to the bulk, confirmed by MD (see Fig. S1 in the ESI†), and considered as a metastable structure. According to previous reports, surface V_I should be a stronger recombination center because it has a large atomic relaxation.[41–43]

It is noteworthy that despite the comparable energy values of the aforementioned defects, Fig. 1(e–g), their spontaneous transitions are not observed during the structural optimization, hinting at their potential coexistence in practical applications. To unravel the difficulty of defect transition, we then assessed migration barriers and found that the transition between surface and subsurface layers needs to overcome an energy barrier of less than 200 meV (Fig. 1e and f), apparently lower than that of an OIHP.[33] This can be traced to the absence of hydrogen bonding between organic cations and iodine in $CsPbI_3$. Such a small migration barrier portends potential issues, such as (i) rapid phase transformations. For example, Guo *et al.* proved theoretically that V_I can trigger a domino effect leading to the $CsPbI_3$ transformation from a perovskite to non-perovskite phase.[44] This reflects that the phase transition of $CsPbI_3$ is relatively fast because of a low migration barrier, compared with that of OIHPs; (ii) surface reconstruction; and (iii) alterations in electronic structures and device performance. In this work, we focus on the latter two aspects. Subsurface defects exhibit an even lower transition barrier of 60 meV, indicating that the thermal effect suffices for conversion. This is also supported by the evolution of bond lengths between Pb1 and Pb2 *via* MD simulations (Fig. S1†).

The detailed analysis of static electronic structures offers fundamental insights into carrier behavior and materials properties, contributing to comprehending e–h recombination dynamics. Fig. 2a illustrates the projected density of states (pDOS) of perfect $CsPbI_3$-(001) surface that is split into Cs, Pb, and I contributions. Specifically, the VBM and CBM are predominantly attributed to I and Pb atoms, respectively, as demonstrated by charge density in the illustration. This spatial separation of VBM and CBM charge densities minimizes their overlap, thereby weakening the e–h interaction and slowing down the charge recombination rate. Interestingly, inorganic Cs cations exhibit no direct influence on the electronic band edges, implying that Cs groups solely contribute to stabilizing the PbI_6 octahedra and neutralizing the system, without affecting the charge recombination.

The defect in a crystal usually introduces the corresponding DS in its electronic structure. For neutral V_I, the DS is occupied by an electron, acting as an n-type dopant, so it is located near the CBM.[45] The pDOS of V_I^{Sur} shows that DS does not emerge within the bandgap but resonates with CB (Fig. 2b), similar to OIHPs.[33] Given the single electron occupation of DS, we performed the spin-polarized calculations for the electronic structures (Fig. S2†), further confirming the absence of a defect-free

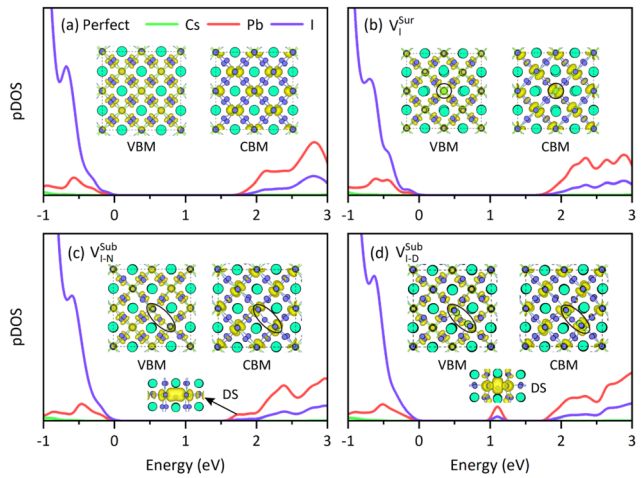

Fig. 2 Projected density of states (pDOS) for (a) perfect $CsPbI_3$ surface, (b) surface layer V_I, and (c) Pb-nondimer and (d) Pb-dimer structures in the subsurface. The insets show charge densities of band edge and defect states. Circles and ovals indicate the location of V_I.

state within the band gap, validating our earlier conclusions. Meanwhile, DS can be demonstrated by two key aspects: (i) charge density distribution. The charge densities of both the DS and CB show that they have similar charge distribution (Fig. S3b†). (ii) Energy-level fluctuations observed in MD simulation, where DS resonates with the CBM (Fig. 3b), in agreement with pDOS analysis results. Intriguingly, this is different from the bulk phase that is shallow-level defect.[45] According to the previous experiences on the carrier dynamics for the bulk phase, such DS has generally no apparent effect on the carrier recombination rate.[46]

Unlike the surface layer defect, the geometry for subsurface V_I is similar to that of the bulk, where iodine-deficient atoms generate dangling bonds adjacent to Pb cations. The spacing between Pb ions directly modulates the electrical properties.

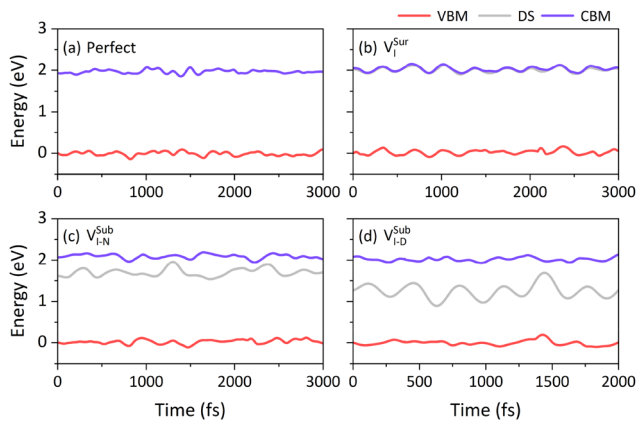

Fig. 3 The time evolution of the VBM, CBM and defect state for $CsPbI_3$-(001) at 300 K. (a–d) Perfect and defective systems. The VBM of the initial configuration is selected for the energy reference. Notably, due to the instability of the subsurface Pb-dimer structure, only a 2 ps trajectory was selected for analysis in this case.

For the Pb-nondimer structure, the reduced distance (5.61 Å) between Pb ions with the dangling enhances their weak interaction, pushing the ppσ state away from the CBM, transforming it into a localized DS.[41] This localized state, commonly referred to as a trap state,[46] is occupied by a single electron, enabling it to capture holes. Consequently, holes generated in the VB upon photoexcitation can recombine with electrons in the DS and CB, as illustrated in Fig. 5b. This phenomenon is intensified in the Pb-dimer structure, where the shortened Pb ion spacing (3.79 Å) pushes the DS into the middle of the bandgap, primarily contributed by Pb ions in the dimer configuration (see charge density in Fig. 2d).

Considering that perovskite cells actually operate at room temperature (300 K), the temperature effect cannot be ignored. Moreover, electron–phonon coupling (EPC) at a finite temperature alters electronic structures and regulates the carrier recombination rate. To this end, we present the evolution of both the band-edges and defect levels at 300 K. Remarkably, the DS in V_I^{Sur} remains in resonance with the CB, which indicates that the recombination process of photogenerated carriers could be a direct recombination of e–h pairs between the band edges. Subsurface V_I, however, introduce the deep-level DS within the band gap. Furthermore, compared with the band edges, the energy-level fluctuation of DS is particularly prominent along the MD trajectory, especially in Pb-dimers. This behavior is somewhat anticipated, as Pb ions near V_I have greater spatial freedom and weaker bonding interactions, leading to more vigorous motions under the thermal influence compared to their lattice atoms.

Fig. 2 and 3 clearly illustrate that the electronic structure of V_I defects on the $CsPbI_3$ surface is strongly influenced by their position, dictated by the growth conditions and ion diffusion. As V_I migrate from the surface to subsurface layer, the Pb–Pb bond length diminishes, particularly when forming the Pb-dimer structure. This shortening enhances the hybridization of Pb-6p orbitals adjacent to V_I (Fig. 2c and d), resulting in a shift of the bonding state ppσ from within the CB towards the band edge, or even deeper into the band gap. These alterations considerably impact carrier capture and relaxation processes, potentially expediting recombination and ultimately modulating the photoelectric properties of the material.

To delve deeper into the role of phonons in electron transitions, we calculated the autocorrelation functions (ACF) and their Fourier transforms (FT) for energy differences between key state pairs along MD trajectories, as shown in Fig. 4. The FT spectrum, also commonly called spectral density, describes the phonon mode participation in the NA carrier relaxation process. The intensity and width of each peak in the spectral density reflect EPC strength at the specific phonon frequency. The results show that the broad phonon modes, including the vibrations of the inorganic Pb–I lattice framework and Cs cations, reflect strong coupling with the electronic subsystem. While Cs cations do not directly impact band edges or defect states, they indirectly affect electrons and holes through electrostatic interactions. From Fig. 4, we observe that: (i) the main peaks below 400 cm^{-1} are attributed to the stretching

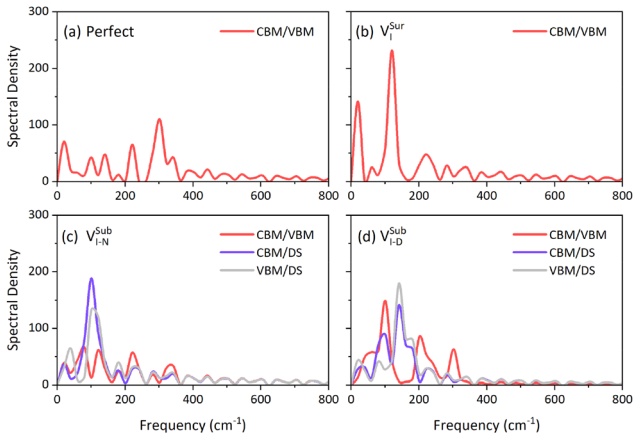

Fig. 4 Spectral densities obtained from the Fourier transform of the autocorrelation functions for the energy gap fluctuation of the pairwise electronic states on (a) perfect $CsPbI_3$ surface, (b) surface layer V_I, and (c) Pb-nondimer and (d) Pb-dimer structures on the subsurface. The *y*-axis represents the amplitude, with no units.

and bending modes of the Pb–I lattice in the PbI_6 octahedra,[47] which supports the capture and recombination processes of carriers. In contrast, higher frequency phonon modes are scarce due to Cs cation disengagement. This is in agreement with previous results obtained from Raman spectroscopy and theoretical calculations.[48–50] (ii) V_I^{Sur} hardly alters band-edge electronic properties (Fig. 2 and 3) but notably enhances low-frequency Pb–I bending modes, as evidenced by increased NAC values shown in Table 1. (iii) Subsurface V_I create localized states within the band gap, leading to more complex vibration modes and a shift toward high frequencies. Phonon modes between the defect and band-edge states exhibit higher intensity and broader widths compared with those between the band-edge states, suggesting a more obvious carrier relaxation process in the former case. Overall, V_I defects indeed modulate the carrier dynamics and accelerate recombination, thereby directly affecting the material performance.

Table 1 Averaged absolute value of NAC (meV), pure-daphasing time (fs), and relaxation lifetime (ns) for the pairwise states in perfect and defective systems. For systems with DS in the bandgap, the values in parentheses denote the overall e–h recombination lifetime. In contrast, for systems without such states, it represents the relaxation lifetime from the CBM to VBM

System	Channel	NAC	Dephasing	Lifetime
Perfect	CBM → VBM	0.20	11.3	141.8
V_I^{Sur}	CBM → VBM	0.29	12.7	73.7
$V_{I\text{-}N}^{Sub}$	CBM → VBM	0.31	11.7	73.5 (21.6)
	CBM → DS	0.43	6.7	1.05
	VBM → DS	0.22	7.0	29.3
$V_{I\text{-}D}^{Sub}$	CBM → VBM	0.30	9.5	40.8 (10.7)
	CBM → DS	0.33	4.2	2.46
	VBM → DS	0.21	4.6	10.8
Pas-V_I^{Sur}	CBM → VBM	0.24	17.5	110.4
Pas-V_I^{Sub}	CBM → VBM	0.23	13.1	115.3

EPC plays a key role in the carrier dynamics of perovskites, because it induces both elastic and inelastic electron scattering. Elastic scattering disrupts the quantum coherence within the electronic subsystem, while the inelastic scattering dissipates electronic energy into heat through nonradiative e–h relaxation, determining optical linewidths.[51,52] To quantify this, we calculated pure-dephasing time using the second-order cumulant approximation.[53–55] This time scale is around 10 fs, much shorter than the time scale of e–h recombination (nanoseconds).[56] Therefore, it is necessary to account for the decoherence effect in NAMD simulations. In general, a short-lived superposition state can prolong the carrier lifetime in perovskites due to the quantum Zeno effect,[57] offering insight into their exceptional excited-state lifetime and high PCE.

Upon photoexcitation, EPC can prompt direct recombination between electrons in the CBM and holes in the VBM (Fig. 5a), or indirect recombination assisted by DS (Fig. 5b). The introduction of DS dramatically complicates the e–h pair recombination process. The carrier lifetime τ (recombination rate, $1/\tau$) of these paired states is obtained by fitting the data with an exponential function, $p(\tau) = \exp(-t/\tau)$, where $p(\tau)$ is the population evolution. The corresponding results are shown in Table 1, including NAC and relaxation lifetime between paired states and overall lifetime. Among them, the overall lifetime involving multiple dynamic processes is obtained by solving the kinetic equations with multiple recombination rates (see the ESI† for computational details), and the results are illustrated in Fig. 5(c–f).

For a perfect surface, the calculated e–h recombination lifetime is 141.8 ns, consistent with an experimental report.[13] Such a long lifetime can be attributed to the relatively weak NAC strength (0.20 meV) and faster decoherence time (11.3 fs). The underlying reason is the fact that the wavefunctions of the two electronic states (VBM and CBM) are mainly localized to different atoms (Fig. 2a). In contrast, the introduction of V_I^{Sur}, even without an additional defect state within the band gap and with localized band-edge wavefunctions (Fig. 2b), substan-

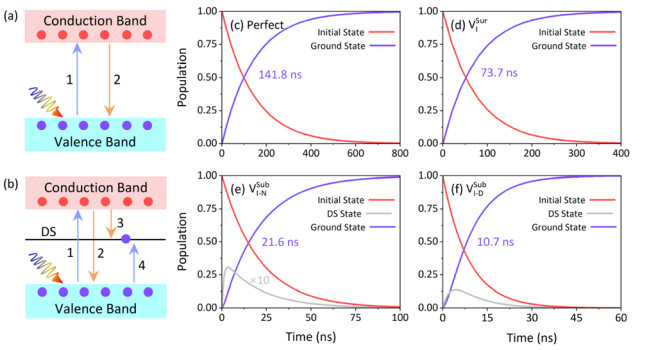

Fig. 5 Electron–hole recombination channels without (a) and with (b) the defect states: (1) Formation of photoexcited electrons and holes. (2) Direct non-radiative recombination between electrons in the CBM and holes in the VBM. (3) Capture of holes by the defect states. (4) Recombination of the trapped holes with electrons in the CBM. (c–f) Population evolution of key states for charge trapping and recombination in perfect and defective $CsPbI_3$.

tially modifies both NAC and decoherence time, especially increasing NAC (0.29 meV). This enhancement, evident in the spectral density (Fig. 4b), stems from intensified low-frequency phonon modes. As a result, the excited-state lifetime of V_I^{Sur} is shortened to 73.7 ns, similar to the recombination behaviors of the bulk system.[45] Therefore, V_I^{Sur} act as an effective recombination center in $CsPbI_3$, supporting experimental observations that V_I defect passivation is crucial for improving device performance.

The subsurface V_I defects markedly accelerate e–h recombination, mainly due to the presence of localized DS in the band gap. The hole capture time for these defect states is significantly shorter than the band edges (29.3 ns *vs.* 73.5 ns for $V_{I\text{-}N}^{Sub}$, 10.8 ns *vs.* 40.8 ns for $V_{I\text{-}D}^{Sub}$, Table 1), indicating that a faster trapping channel for holes is provided. Once trapped, the holes recombine with electrons in the CB within 3 ns (CBM → DS). Thus, the DS population does not continuously increase but rather exhibits a transient rise followed by a decay process (Fig. 5e and f). For $V_{I\text{-}N}^{Sub}$, the calculated lifetime of the excited electrons in the CB is 21.6 ns, and the recombination rate of e–h pairs is increased by 6.5 times and 3.4 times, respectively, compared with the perfect and V_I^{Sur} systems. When subsurface defect forms the Pb-dimer configuration, the carrier lifetime further decreases to 10.7 ns, due to a shorter capture hole lifetime (VBM → DS) of 10.8 ns compared to 29.3 ns for the Pb-nondimer case. This reduction stems from the narrower energy gap between the VBM and DS. Our results indicate that the DS introduced by the V_I defect diminishes the direct e–h recombination at band edges, favoring recombination assisted by the DS instead. This is evident from the much longer lifetime of direct recombination compared to the total excited electron lifetime (73.5 ns *vs.* 21.6 ns for $V_{I\text{-}N}^{Sub}$, 40.8 ns *vs.* 10.7 ns for $V_{I\text{-}D}^{Sub}$, see Table 1 and Fig. 5, respectively), suggesting that DS greatly increases energy dissipation through heat generation. These findings indicate that V_I defects near the surface are detrimental to halide perovskites, and their reduction can effectively boost the PCE. This perspective is supported by experimental works, which have revealed that cell performance can be notably improved by moving surface defects.[8,23] In addition, the analysis of carrier lifetime, combined with the previous discussion on ionic diffusion, elucidates why the PCE of $CsPbI_3$ generally lags behind that of OIHPs. One important reason is the low diffusion energy barriers on the surface and corresponding shorter carrier lifetime in $CsPbI_3$.

An efficient and prevalent approach for reducing surface V_I is to modify surfaces with passivating agents based on the Lewis acid–base reaction principle. This strategy can enhance both efficiency and stability of perovskites. Compared to other Lewis base molecules, the passivator $HCOO^-$ has a higher adsorption energy and can form stable Pb–O coordination bonds with the unsaturated Pb ions.[12,18,58] Therefore, here we chose the $HCOO^-$ anions to further investigate their regulatory effect on surface and subsurface V_I defects. Fig. 6(a and b) depict the optimized geometries of $HCOO^-$ passivating surface and subsurface layer V_I, named Pas-V_I^{Sur} and Pas-V_I^{Sub}, respectively. Notably, when $HCOO^-$ anions interact with $V_{I\text{-}D}^{Sub}$, their strong absorption energy (about 4 eV) spontaneously disrupts the weak Pb-dimer bond and then transforms into a more stable Pb-nondimer structure. To substantiate $HCOO^-$ passivation efficacy at 300 K, MD simulations reveal the Pb–Pb bond lengths over time (see Fig. S8 in the ESI†), confirming its ability to stabilize surface V_I defects. In addition, the average bond lengths of Pb–O (2.66 Å at the surface, 2.56 Å at the subsurface) are comparable to the sum of Pb and O radii (2.41 Å), demonstrating the strong bonding capacity of $HCOO^-$. This capacity can inhibit V_I migration and defect reconstruction, thereby bolstering the structural stability of perovskites.

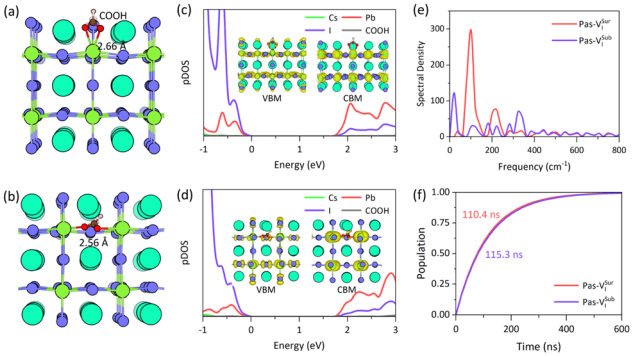

Fig. 6 Optimized geometry of $HCOO^-$ anions passivating surface (a) and subsurface (b) iodine vacancy defects. (c and d) pDOS of (a) and (b) systems, respectively, and the illustrations show the charge density for the VBM and CBM. (e) Spectral densities obtained by Fourier transform of the autocorrelation functions of band gap fluctuations for these systems. (f) Carrier dynamics for the excited state in (a) and (b), respectively.

Upon introducing the $HCOO^-$ passivator, the VBM and CBM are still primarily contributed by I and Pb atoms, while $HCOO^-$ anions have a negligible effect on the band edges, and do not introduce new defect states within the band gap, as shown in Fig. 6(c and d). For subsurface defects, the passivator $HCOO^-$ effectively eliminates the initially strongly localized DS within the band gap, as depicted in Fig. 5a, inhibiting rapid e–h recombination *via* DS and extending the excited-state carrier lifetime. The FT of the energy difference between the VBM and CBM (Fig. 6e) shows that low-frequency phonon modes dominate the spectral density, consistent with Fig. 4. Notably, $HCOO^-$ significantly weakens the phonon vibrations and intensities originating from the inorganic sublattice, compared to the unpassivated defect, as evidenced by reduced peak numbers and values, indicating a decrease in EPC (Table 1). These effects synergistically regulate carrier lifetime, as illustrated by the population evolution in Fig. 6f. With post-passivation, the carrier lifetime of surface and subsurface layer V_I defects is 110.4 ns and 115.3 ns, respectively, marking a substantial improvement in defect systems. The prolonged lifetime is attributed to the reduced NAC strength, shorter decoherence time, and the elimination of the in-gap defect state, as detailed in Table 1 and Fig. 6. These calculations provide direct evidence that passivators with Lewis base functional

groups can effectively mitigate the detrimental V_I defects near the surface, even for shallow-level or resonant V_I^{Sur} defects.

It has been reported that surface modification with Lewis base molecules can extend charge carrier lifetime, thereby boosting PCE and stability. Nenon *et al.* utilized ^{1}H NMR spectroscopy to identify surface halide vacancies in $CsPbX_3$ (X = Cl, Br, and I) as the primary source of charge trapping, revealing that X-type Lewis bases effectively passivated these defects, dramatically enhancing lifetime and PLQY.[15] Xiong *et al.* crafted MPA molecules that forged strong P–O–Pb covalent bonds with surface V_I in $CsFAPb(I,Br)_3$, and diminished defect concentration. This refinement elevated the lifetime from 4.15 ns to 7.92 ns, and attained a stable PCE of 25.53%, retaining ~95% initial efficiency after 1000 hours.[59] Gu *et al.* discovered that HA molecules effectively engage with the abundant V_I on the surface of $CsPbI_{1-x}Br_x$, reducing the number of uncoordinated Pb^{2+} and Pb clusters, and achieve a champion PCE of 20.8% under 100 mW cm^{-2} illumination.[11] Our results rationalize these experimental observations and further emphasize the paramount importance of surface defect passivation for realizing high-performance PSCs.

Conclusions

In summary, we employed a suite of computational approaches to comprehensively study the diffusion barriers, electronic structures, charge captures and recombination mechanisms of V_I in various configurations near the surface of all-inorganic $CsPbI_3$. Our findings reveal that V_I defects, both on the outermost and subsurface layers, possess equivalent energies and do not spontaneously transform during structural relaxation, hinting at their potential coexistence. The transitions between these defects involve relatively low energy barriers, lower than those in OIHPs, suggesting that $CsPbI_3$ is more prone to the surface defect reconstruction. Electronic structures and carrier dynamics show that despite surface layer V_I acting as a resonant defect, it drastically reduces the carrier lifetime due to strong EPC, while subsurface V_I defects introduce new localized DS in the bandgap, providing additional e–h recombination channels, particularly in the Pb-dimer configuration, which accelerates hole capture because of a small gap between the VBM and DS. These discoveries support the experimental observations that V_I defects on the perovskite surfaces are detrimental. By introducing the passivator $HCOO^-$, we demonstrate its effectiveness in passivating the DS, weakening EPC, and extending the excited state lifetime by an order of magnitude. This study sheds light on the mechanistic effects of Lewis base passivators on the carrier recombination dynamics in perovskites, and offers novel insights for enhancing carrier lifetime and PCE.

Author contributions

J. W. conceived and supervised the project, and performed the DFT calculations. J. W. and X-M. D. analysed the data and co-wrote the paper.

Data availability

The authors confirm that the data supporting the findings of this study are available within the article or its ESI.† In addition, it may be obtained from the corresponding author, upon reasonable request.

Conflicts of interest

There are no conflicts to declare.

Acknowledgements

This work was funded by the National Natural Science Foundation of China (Grant No. 12204256 and 12147121) and supported by the Ningbo Yongjiang Talent Programme of China (2023A-156-G). DFT simulations were carried out at the Supercomputer Center of NBU.

References

1 G. E. Eperon, G. M. Paternò, R. J. Sutton, A. Zampetti, A. A. Haghighirad, F. Cacialli and H. J. Snaith, Inorganic caesium lead iodide perovskite solar cells, *J. Mater. Chem. A*, 2015, **3**, 19688–19695.
2 J. Wang, Y. Che, Y. Duan, Z. Liu, S. Yang, D. Xu, Z. Fang, X. Lei, Y. Li and S. F. Liu, 21.15%-Efficiency and Stable gamma -$CsPbI_3$ Perovskite Solar Cells Enabled by an Acyloin Ligand, *Adv. Mater.*, 2023, **35**, e2210223.
3 S. Yang, M. Wu, X. Lei, J. Wang, Y. Han, X. He, S. Liu and Z. Liu, Ultra-High 1.27 V VOC of Pure $CsPbI_3$ Perovskite Solar Cells with an Efficiency of 21.8%, *ACS Energy Lett.*, 2024, **9**, 4817–4826.
4 S. S. Mali, J. V. Patil, J.-Y. Shao, Y.-W. Zhong, S. R. Rondiya, N. Y. Dzade and C. K. Hong, Phase-heterojunction all-inorganic perovskite solar cells surpassing 21.5% efficiency, *Nat. Energy*, 2023, **8**, 989–1001.
5 *Best Research-Cell Efficiencies*. **https://www.nrel.gov/pv/device-performance.html**.
6 S. Rühle, Tabulated values of the Shockley–Queisser limit for single junction solar cells, *Sol. Energy*, 2016, **130**, 139–147.
7 B. Wu, H. T. Nguyen, Z. Ku, G. Han, D. Giovanni, N. Mathews, H. J. Fan and T. C. Sum, Discerning the Surface and Bulk Recombination Kinetics of Organic-Inorganic Halide Perovskite Single Crystals, *Adv. Energy Mater.*, 2016, **6**, 1600551.
8 Z. Ni, C. Bao, Y. Liu, Q. Jiang, W.-Q. Wu, S. Chen, X. Dai, B. Chen, B. Hartweg and Z. Yu, Resolving spatial and energetic distributions of trap states in metal halide perovskite solar cells, *Science*, 2020, **367**, 1352–1358.
9 J. Huang, Y. Yuan, Y. Shao and Y. Yan, Understanding the physical properties of hybrid perovskites for photovoltaic applications, *Nat. Rev. Mater.*, 2017, **2**, 1–19.

10 F. Ambrosio, D. Meggiolaro, E. Mosconi and F. De Angelis, Charge localization and trapping at surfaces in lead-iodide perovskites: the role of polarons and defects, *J. Mater. Chem. A*, 2020, **8**, 6882–6892.
11 X. Gu, W. Xiang, Q. Tian and S. F. Liu, Rational Surface-Defect Control via Designed Passivation for High-Efficiency Inorganic Perovskite Solar Cells, *Angew. Chem., Int. Ed.*, 2021, **60**, 23164–23170.
12 L. He, G. Hu, J. Jiang, W. Wei, X. Xue, K. Fan, H. Huang and L. Shen, Highly Sensitive Tin-Lead Perovskite Photodetectors with Over 450 Days Stability Enabled by Synergistic Engineering for Pulse Oximetry System, *Adv. Mater.*, 2023, **35**, e2210016.
13 R. Li, S. Zhang, H. Zhang, Z. Wang, X. Feng, Y. Du, T. Zhou, X. Chen, P. Liu, L. Liu, J. Zhang, Q. Chen, L. Xi, K. Zhao, S. F. Liu and Q. Tian, Customizing Aniline-Derived Molecular Structures to Attain beyond 22% Efficient Inorganic Perovskite Solar Cells, *Angew. Chem., Int. Ed.*, 2024, e202410600.
14 H. Uratani and K. Yamashita, Charge Carrier Trapping at Surface Defects of Perovskite Solar Cell Absorbers: A First-Principles Study, *J. Phys. Chem. Lett.*, 2017, **8**, 742–746.
15 D. P. Nenon, K. Pressler, J. Kang, B. A. Koscher, J. H. Olshansky, W. T. Osowiecki, M. A. Koc, L. W. Wang and A. P. Alivisatos, Design Principles for Trap-Free $CsPbX_3$ Nanocrystals: Enumerating and Eliminating Surface Halide Vacancies with Softer Lewis Bases, *J. Am. Chem. Soc.*, 2018, **140**, 17760–17772.
16 W. Shockley and W. T. Read, Statistics of the Recombinations of Holes and Electrons, *Phys. Rev.*, 1952, **87**, 835–842.
17 R. N. Hall, Electron-Hole Recombination in Germanium, *Phys. Rev.*, 1952, **87**, 387–387.
18 J. Xu, H. Chen, L. Grater, C. Liu, Y. Yang, S. Teale, A. Maxwell, S. Mahesh, H. Wan, Y. Chang, B. Chen, B. Rehl, S. M. Park, M. G. Kanatzidis and E. H. Sargent, Anion optimization for bifunctional surface passivation in perovskite solar cells, *Nat. Mater.*, 2023, **22**, 1507–1514.
19 R. Wang, J. Xue, K.-L. Wang, Z.-K. Wang, Y. Luo, D. Fenning, G. Xu, S. Nuryyeva, T. Huang, Y. Zhao, J. L. Yang, J. Zhu, M. Wang, S. Tan, I. Yavuz, K. N. Houk and Y. Yang, Constructive molecular configurations for surface-defect passivation of perovskite photovoltaics, *Science*, 2019, **366**, 1509–1513.
20 T. Wang, Y. Li, Q. Cao, J. Yang, B. Yang, X. Pu, Y. Zhang, J. Zhao, Y. Zhang, H. Chen, A. Hagfeldt and X. Li, Deep defect passivation and shallow vacancy repair via an ionic silicone polymer toward highly stable inverted perovskite solar cells, *Energy Environ. Sci.*, 2022, **15**, 4414–4424.
21 X. Yang, Y. Ni, Y. Zhang, Y. Wang, W. Yang, D. Luo, Y. Tu, Q. Gong, H. Yu and R. Zhu, Multiple-Defect Management for Efficient Perovskite Photovoltaics, *ACS Energy Lett.*, 2021, **6**, 2404–2412.
22 W.-T. Wang, P. Holzhey, N. Zhou, Q. Zhang, S. Zhou, E. A. Duijnstee, K. J. Rietwyk, J.-Y. Lin, Y. Mu, Y. Zhang, U. Bach, C.-G. Wu, H. L. Yip, H. J. Snaith and S.-P. Feng, Water- and heat-activated dynamic passivation for perovskite photovoltaics, *Nature*, 2024, **632**, 294–300.
23 Y. Pan, J. Wang, Z. Sun, J. Zhang, Z. Zhou, C. Shi, S. Liu, F. Ren, R. Chen, Y. Cai, H. Sun, B. Liu, Z. Zhang, Z. Zhao, Z. Cai, X. Qin, Z. Zhao, Y. Ji, N. Li, W. Huang, Z. Liu and W. Chen, Surface chemical polishing and passivation minimize non-radiative recombination for all-perovskite tandem solar cells, *Nat. Commun.*, 2024, **15**, 7335.
24 G. Kresse and J. Furthmüller, Efficiency of *ab initio* total energy calculations for metals and semiconductors using a plane-wave basis set, *Comput. Mater. Sci.*, 1996, **6**, 15–50.
25 G. Kresse and J. Furthmüller, Efficient iterative schemes for ab initio total-energy calculations using a plane-wave basis set, *Phys. Rev. B:Condens. Matter Mater. Phys.*, 1996, **54**, 11169.
26 G. Kresse and D. Joubert, From ultrasoft pseudopotentials to the projector augmented-wave method, *Phys. Rev. B: Condens. Matter Mater. Phys.*, 1999, **59**, 1758.
27 J. P. Perdew, K. Burke and M. Ernzerhof, Generalized gradient approximation made simple, *Phys. Rev. Lett.*, 1996, **77**, 3865.
28 H. J. Monkhorst and J. D. Pack, Special points for Brillouin-zone integrations, *Phys. Rev. B*, 1976, **13**, 5188.
29 I. Deretzis, C. Bongiorno, G. Mannino, E. Smecca, S. Sanzaro, S. Valastro, G. Fisicaro, A. La Magna and A. Alberti, Exploring the Structural Competition between the Black and the Yellow Phase of $CsPbI_3$, *Nanomaterials*, 2021, **11**, 1282.
30 J. A. S. Laranjeira, S. A. Azevedo, G. S. L. Fabris, J. R. Sambrano and M. M. Ferrer, Surface stability and morphological transformations of $CsPbI_3$, *Comput. Mater. Sci.*, 2024, **239**, 112977.
31 Y. Guo, C. Li, X. Li, Y. Niu, S. Hou and F. Wang, Effects of Rb Incorporation and Water Degradation on the Stability of the Cubic Formamidinium Lead Iodide Perovskite Surface: A First-Principles Study, *J. Phys. Chem. C*, 2017, **121**, 12711–12717.
32 Y. Yang, F. Gao, S. Gao and S.-H. Wei, Origin of the stability of two-dimensional perovskites: a first-principles study, *J. Mater. Chem. A*, 2018, **6**, 14949–14955.
33 J. Wang and W. J. Yin, Revisiting the Iodine Vacancy Surface Defects to Rationalize Passivation Strategies in Perovskite Solar Cells, *J. Phys. Chem. Lett.*, 2022, **13**, 6694–6700.
34 S. Grimme, J. Antony, S. Ehrlich and H. Krieg, A consistent and accurate ab initio parametrization of density functional dispersion correction (DFT-D) for the 94 elements H-Pu, *J. Chem. Phys.*, 2010, **132**, 154104.
35 G. Henkelman, B. P. Uberuaga and H. Jónsson, A climbing image nudged elastic band method for finding saddle points and minimum energy paths, *J. Chem. Phys.*, 2000, **113**, 9901–9904.
36 N. Shuichi, Constant temperature molecular dynamics methods, *Prog. Theor. Phys. Suppl.*, 1991, **103**, 1–46.

37 A. V. Akimov and O. V. Prezhdo, The PYXAID program for non-adiabatic molecular dynamics in condensed matter systems, *J. Chem. Theory Comput.*, 2013, **9**, 4959–4972.
38 A. V. Akimov and O. V. Prezhdo, Advanced capabilities of the PYXAID program: integration schemes, decoherence effects, multiexcitonic states, and field-matter interaction, *J. Chem. Theory Comput.*, 2014, **10**, 789–804.
39 P. Giannozzi, S. Baroni, N. Bonini, M. Calandra, R. Car, C. Cavazzoni, D. Ceresoli, G. L. Chiarotti, M. Cococcioni and I. Dabo, QUANTUM ESPRESSO: a modular and open-source software project for quantum simulations of materials, *J. Phys.: Condens. Matter*, 2009, **21**, 395502.
40 H. M. Jaeger, S. Fischer and O. V. Prezhdo, Decoherence-induced surface hopping, *J. Chem. Phys.*, 2012, **137**, 22A545.
41 J. Wang, W. Li and W. J. Yin, Passivating Detrimental DX Centers in $CH_3NH_3PbI_3$ for Reducing Nonradiative Recombination and Elongating Carrier Lifetime, *Adv. Mater.*, 2020, **32**, e1906115.
42 J. Li, H.-F. Zhu, Y.-Y. Zhang, Z.-K. Yuan, S. Chen and X.-G. Gong, Large carrier-capture rate of PbI antisite in $CH_3NH_3PbI_3$ induced by heavy atoms and soft phonon modes, *Phys. Rev. B*, 2017, **96**, 104103.
43 J. Li, Z.-K. Yuan, S. Chen, X.-G. Gong and S.-H. Wei, Effective and Noneffective Recombination Center Defects in Cu_2ZnSnS_4: Significant Difference in Carrier Capture Cross Sections, *Chem. Mater.*, 2019, **31**, 826–833.
44 Z. Guo, J. Fu, G. Chen, F. Liu, C. Yu, R. Lu and W. J. Yin, First Domino in the Structural Collapse of Perovskite $CsPbI_3$ and Its Stabilizing Strategies, *Adv. Funct. Mater.*, 2023, **34**, 2308246.
45 W. Li, Y. Y. Sun, L. Li, Z. Zhou, J. Tang and O. V. Prezhdo, Control of Charge Recombination in Perovskites by Oxidation State of Halide Vacancy, *J. Am. Chem. Soc.*, 2018, **140**, 15753–15763.
46 J. Wang and X.-M. Duan, Defect engineering of $CH_3NH_3PbI_3$ towards enhanced carrier lifetime: combined detailed balanced study and NAMD-TDDFT, *Inorg. Chem. Front.*, 2024, **11**, 6467–6475.
47 Y. Yang, J. P. Robbins, L. Ezeonu, Y. Ma, N. Sparta, X. Kong, S. Strauf, S. G. Podkolzin and S. S. Lee, Probing lattice vibrations of stabilized $CsPbI_3$ polymorphs via low-frequency Raman spectroscopy, *J. Mater. Chem. C*, 2020, **8**, 8896–8903.
48 A. Ren, H. Lai, X. Hao, Z. Tang, H. Xu, B. M. F. Yu Jeco, K. Watanabe, L. Wu, J. Zhang, M. Sugiyama, J. Wu and D. Zhao, Efficient Perovskite Solar Modules with Minimized Nonradiative Recombination and Local Carrier Transport Losses, *Joule*, 2020, **4**, 1263–1277.
49 P. Nandi, C. Giri, B. Joseph, S. Rath, U. Manju and D. Topwal, $CH_3NH_3PbI_3$, A Potential Solar Cell Candidate: Structural and Spectroscopic Investigations, *J. Phys. Chem. A*, 2016, **120**, 9732–9739.
50 J. Wang and W.-J. Yin, Effect of alloying on the carrier dynamics in high-performance perovskite solar cells, *J. Energy Chem.*, 2022, **68**, 267–274.
51 J. Liu, S. V. Kilina, S. Tretiak and O. V. Prezhdo, Ligands slow down pure-dephasing in semiconductor quantum dots, *ACS Nano*, 2015, **9**, 9106–9116.
52 S. Pal, P. Nijjar, T. Frauenheim and O. V. Prezhdo, Atomistic Analysis of Room Temperature Quantum Coherence in Two-Dimensional CdSe Nanostructures, *Nano Lett.*, 2017, **17**, 2389–2396.
53 S. Mukamel, *Principles of Nonlinear Optical Spectroscopy: Oxford Series in Optical and Imaging Sciences*, Oxford University Press, New York, 1995.
54 A. V. Akimov and O. V. Prezhdo, Persistent Electronic Coherence Despite Rapid Loss of Electron–Nuclear Correlation, *J. Phys. Chem. Lett.*, 2013, **4**, 3857–3864.
55 H. Kamisaka, S. V. Kilina, K. Yamashita and O. V. Prezhdo, Ab initio study of temperature and pressure dependence of energy and phonon-induced dephasing of electronic excitations in CdSe and PbSe quantum dots, *J. Phys. Chem. C*, 2008, **112**, 7800–7808.
56 Z. Guo, X. Wu, T. Zhu, X. Zhu and L. Huang, Electron-Phonon Scattering in Atomically Thin 2D Perovskites, *ACS Nano*, 2016, **10**, 9992–9998.
57 S. V. Kilina, A. J. Neukirch, B. F. Habenicht, D. S. Kilin and O. V. Prezhdo, Quantum zeno effect rationalizes the phonon bottleneck in semiconductor quantum dots, *Phys. Rev. Lett.*, 2013, **110**, 180404.
58 J. Jeong, M. Kim, J. Seo, H. Lu, P. Ahlawat, A. Mishra, Y. Yang, M. A. Hope, F. T. Eickemeyer, M. Kim, Y. J. Yoon, I. W. Choi, B. P. Darwich, S. J. Choi, Y. Jo, J. H. Lee, B. Walker, S. M. Zakeeruddin, L. Emsley, U. Rothlisberger, A. Hagfeldt, D. S. Kim, M. Grätzel and J. Y. Kim, Pseudo-halide anion engineering for α-$FAPbI_3$ perovskite solar cells, *Nature*, 2021, **592**, 381–385.
59 S. Xiong, F. Tian, F. Wang, A. Cao, Z. Chen, S. Jiang, D. Li, B. Xu, H. Wu, Y. Zhang, H. Qiao, Z. Ma, J. Tang, H. Zhu, Y. Yao, X. Liu, L. Zhang, Z. Sun, M. Fahlman, J. Chu, F. Gao and Q. Bao, Reducing nonradiative recombination for highly efficient inverted perovskite solar cells via a synergistic bimolecular interface, *Nat. Commun.*, 2024, **15**, 5607.